The Robustness of Midlatitude Weather Pattern Changes due to Arctic Sea Ice Loss

HANS W. CHEN AND FUQING ZHANG

Department of Meteorology and Atmospheric Science, and Center for Advanced Data Assimilation and Predictability Techniques, The Pennsylvania State University, University Park, Pennsylvania

RICHARD B. ALLEY

Department of Geosciences, Earth and Environmental Systems Institute, and Center for Advanced Data Assimilation and Predictability Techniques, The Pennsylvania State University, University Park, Pennsylvania

(Manuscript received 23 February 2016, in final form 26 July 2016)

ABSTRACT

The significance and robustness of the link between Arctic sea ice loss and changes in midlatitude weather patterns is investigated through a series of model simulations from the Community Atmosphere Model, version 5.3, with systematically perturbed sea ice cover in the Arctic. Using a large ensemble of 10 sea ice scenarios and 550 simulations, it is found that prescribed Arctic sea ice anomalies produce statistically significant changes for certain metrics of the midlatitude circulation but not for others. Furthermore, the significant midlatitude circulation changes do not scale linearly with the sea ice anomalies and are not present in all scenarios, indicating that the remote atmospheric response to reduced Arctic sea ice can be statistically significant under certain conditions but is generally nonrobust. Shifts in the Northern Hemisphere polar jet stream and changes in the meridional extent of upper-level large-scale waves due to the sea ice perturbations are generally small and not clearly distinguished from intrinsic variability. Reduced Arctic sea ice may favor a circulation pattern that resembles the negative phase of the Arctic Oscillation and may increase the risk of cold outbreaks in eastern Asia by almost 50%, but this response is found in only half of the scenarios with negative sea ice anomalies. In eastern North America the frequency of extreme cold events decreases almost linearly with decreasing sea ice cover. This study's finding of frequent significant anomalies without a robust linear response suggests interactions between variability and persistence in the coupled system, which may contribute to the lack of convergence among studies of Arctic influences on midlatitude circulation.

1. Introduction

Arctic sea ice is melting at an accelerating rate (Comiso et al. 2008) that is possibly unprecedented over at least the past few millennia (Kinnard et al. 2011; Polyak et al. 2010). Sea ice plays a central role in the local climate system through its influence on surface albedo, heat and moisture fluxes between the atmosphere and ocean, surface friction, and ocean circulation. Decreased sea ice coverage is one of the main drivers of Arctic amplification (Screen and Simmonds 2010)—that is, larger surface warming in the Arctic relative to the rest of the globe—a phenomenon that is evident in both observations and future climate projections (IPCC 2013; Serreze and Francis 2006). Whether the sea ice anomalies in the Arctic are having or will have major effects on climate at lower latitudes remains uncertain (Wallace et al. 2014) but is of great importance for our understanding of future climate change impacts, as the Arctic sea ice cover is most likely going to continue to decrease in the near future (IPCC 2013).

The atmospheric response to Arctic sea ice loss has been investigated in numerous studies (see, e.g., Cohen et al. 2014; Vihma 2014; Walsh 2014, and references therein). Francis and Vavrus (2012) proposed that Arctic amplification and the associated decrease in

Corresponding author address: Hans W. Chen, Department of Meteorology and Atmospheric Science, and Center for Advanced Data Assimilation and Predictability Techniques, The Pennsylvania State University, 624 Walker Building, University Park, PA 16802.
E-mail: hans.chen@psu.edu

DOI: 10.1175/JCLI-D-16-0167.1

meridional thickness gradient has contributed to an increased meandering upper-level flow and slower progression of weather systems in the midlatitudes, which could result in more frequent blocking patterns and extreme weather events such as droughts and heat waves. In a subsequent study, Francis and Vavrus (2015) found evidence for a wavier jet stream in observations linked to Arctic warming and sea ice loss. However, other studies have shown that observed trends in planetary wave amplitude linked to sea ice loss and extreme weather events can be sensitive to the methodology (Barnes 2013) and may not be statistically significant in the short time series of observations (Screen and Simmonds 2013a).

Many modeling studies with forced Arctic sea ice reduction have found that decreased sea ice coverage in the Arctic leads to a circulation pattern in winter that projects onto the negative phase of the Arctic Oscillation (AO; Alexander et al. 2004; Deser et al. 2010; Hopsch et al. 2012; Jaiser et al. 2012; Liu et al. 2012; Peings and Magnusdottir 2014; Screen et al. 2013). Contrary to these results, the large-scale atmospheric responses in some modeling studies do not resemble the AO or project onto the positive phase of the AO (e.g., Screen et al. 2014). The reason behind this apparent discrepancy is not well understood, partly because it is difficult to compare different modeling studies because of differences in their methodologies.

One proposed dynamical pathway from reduced Arctic sea ice to anomalous circulation patterns in the midlatitudes is through enhanced upward propagation of planetary waves into the stratosphere, followed by a weakening of the polar vortex (Feldstein and Lee 2014; Kim et al. 2014; Peings and Magnusdottir 2014). This signal projects onto the negative phase of the AO when it reaches the lower levels of the atmosphere. Kim et al. (2014) showed the relationship between reduced sea ice, increased upward propagation of planetary waves, and subsequent weakening of the stratospheric polar vortex using composites of observational data and reproduced some of these signals with two atmospheric models. They found that the decreased sea ice cover in the Barents and Kara Seas played an especially important role for the excitation of upward-propagating waves. Peings and Magnusdottir (2014) used an atmospheric model with prescribed sea ice forcing and demonstrated that the upward propagation of planetary waves does not scale linearly with the sea ice reduction and may actually be weaker for a larger reduction of Arctic sea ice cover compared with moderate sea ice loss.

A growing number of recent studies have stated that the recent loss of Arctic sea ice is linked to a wintertime cooling of the midlatitude continents (Mori et al. 2014; Petoukhov and Semenov 2010; Yang and Christensen 2012) and increased risk of severe winter weather, such as cold outbreaks (Tang et al. 2013) and heavy snowfall (Liu et al. 2012). This link between reduced sea ice coverage and severe cold winters over the midlatitude continents could have major socioeconomic impacts, but large uncertainties about the significance and robustness of these signals remain, with some studies showing a weak or no influence of Arctic sea ice loss (Gerber et al. 2014; Li et al. 2015) or pointing toward an opposite effect of Arctic amplification—for example, reduced temperature variance in northern midlatitudes (Schneider et al. 2015; Screen 2014; Sun et al. 2015) and reduced risk of extreme cold events in North America (Screen et al. 2015a,b).

In spite of recent progress in understanding the links between Arctic sea ice loss and anomalous weather patterns in the midlatitudes, it remains a challenge to draw firm conclusions about the remote impact of reduced Arctic sea ice because of diverse results from different studies. Observational studies are more effective at generating hypotheses than at establishing highly statistically significant relations because of the large variability and relatively short length of available time series (Barnes 2013). Modeling studies, on the other hand, have produced a wide range of results that are sometimes difficult to reconcile. The modeling discrepancies could have arisen from a variety of sources, including the choice of model, model version, coupled model components, initial conditions, horizontal and vertical resolution, treatment of sea surface temperatures (SSTs), and magnitude and spatial pattern of sea ice concentration (SIC) anomalies. Identifying causes of discrepancies between studies is complicated by differences in methodology employed, hindering direct comparison of conflicting results. Part of the discrepancies could be the result of nonlinearity of the atmospheric response with respect to Arctic sea ice anomalies, which has been indicated by previous studies (Peings and Magnusdottir 2014; Perlwitz et al. 2015; Petoukhov and Semenov 2010; Screen and Simmonds 2013a,b; Semenov and Latif 2015), but there is currently no quantification of how robust the remote atmospheric signal is to differences in sea ice perturbations.

The objective of this sensitivity study is to test the significance and robustness of the local and remote atmospheric response to perturbed sea ice cover in the Arctic. We performed a large number of simulations of the atmospheric response to gradually varying sea ice anomalies in the Arctic, in which the atmospheric model was forced with prescribed SIC and SST from 10 different sea ice scenarios. The sea ice scenarios were designed to be consistent and directly comparable. Our sea ice perturbations are largest in September but also persist into the winter months to provide a smooth transition from the September sea ice anomalies. We note that the sea ice perturbations were not created to replicate the sea ice variability during any particular year; thus, one should be careful when comparing the model results with observations. The focus of this study is on the impact of the prescribed Arctic sea ice anomalies on the atmosphere on intra-annual time scales rather than on the long-term equilibrium atmospheric response. Although forced model simulations may not capture all processes related to the atmospheric response (Blackport and Kushner 2016; Deser et al. 2015), the model enables us to assess the response in a controlled setting while varying only the sea ice forcing.

2. Methods

a. Model setup and simulations

We used the latest version of NCAR Community Atmosphere Model [version 5.3 (CAM5); Neale et al. 2012] to examine the atmospheric response across ensembles of simulations for each of a range of Arctic sea ice anomalies. The global atmospheric model was coupled to the Community Land Model (Oleson et al. 2013) and forced with prescribed SIC and SST. The ice thickness was set to a constant value of 2 m. We ran the simulations using the finite volume dynamical core with a horizontal resolution of 1.9° latitude by 2.5° longitude and 30 vertical levels extending up to 3.6 hPa.

A control simulation was created by running the model for 60 years using the climatological mean SIC and SST over 1979–2013. The first 5 years in the control simulation were discarded to account for model spinup, and atmospheric fields from 1 April for the remaining 55 years were used as initial conditions for the ensemble members. Each ensemble member was run for one year with forced SIC and SST boundary conditions.

We simulated the atmospheric response to 10 sea ice scenarios: the unperturbed control scenario, three scenarios with increased Arctic sea ice cover, and six scenarios with decreased sea ice. For each scenario we ran 55 ensemble members, which corresponds to a sample size larger than but on the same order as available observations during the satellite period (about four decades), yielding a total ensemble size of 550 simulations.

b. SIC and SST perturbations

CAM5 takes monthly SIC and SST fields as boundary conditions. During model integration, the model sets the monthly SIC and SST fields as the midmonth values and linearly interpolates the monthly values in time to daily values. In this study we derived the boundary conditions using monthly SIC and SST from the Hadley Centre Sea Ice and Sea Surface Temperature dataset (Rayner 2003) over the 1979–2013 satellite period.

We perturbed the Arctic sea ice cover through a novel method that ensured that the spatial and temporal sea ice variability is realistic and that the sea ice forcings between sea ice scenarios are consistent and directly comparable. The method we used to create new SIC and SST boundary conditions for the perturbed sea ice scenarios can be divided into two steps. First, we perturbed the climatological mean seasonal cycle of Arctic sea ice area to obtain a new seasonal cycle for each sea ice scenario (Fig. 1a). We started off by perturbing the sea ice area in September (the month with the largest observed negative trend in Arctic sea ice area; Simmonds 2015) by a number of climatological standard deviations of September sea ice area, which is denoted by α and ranges from -3 to 3 in our study. Throughout the rest of the paper we will refer to specific sea ice scenarios by their α perturbation. Figure 1b shows how the September sea ice area perturbations in our study compare with observed September sea ice area anomalies between 1979 and 2013. The sea ice areas in the remaining months were then perturbed based on linear regressions between observed sea ice area anomalies in September and the other months. Sea ice area anomalies are thus increased to and decreased from their September maximum anomaly to match persistence of Arctic sea ice area anomalies in observations, and the anomaly in any month is proportional to α. This method provided a smooth transition to the new sea ice state in September. Although we focus on the September sea ice loss, our sea ice area perturbations cover well the range of observed sea ice area anomalies during the summer, autumn, and winter months (Fig. 1a).

In the second step of the sea ice scenario creation process, we found new spatial fields of SIC and SST that match the perturbed monthly mean sea ice areas in Fig. 1a. For each Arctic sea ice season—the melt season (April through September) and freeze season (October through March)—the climatological monthly mean sea ice areas used in the control scenario decrease and increase monotonically with time, respectively; thus, for each season, we can find a unique spatial field of SIC that corresponds to a specific sea ice area by linearly interpolating between the two monthly mean SIC fields in the control scenario with the closest areas, similarly to how the model interpolates the monthly mean SIC fields to daily values. (The main reason we use sea ice area rather than sea ice extent throughout this study is because of this one-to-one correspondence between sea ice

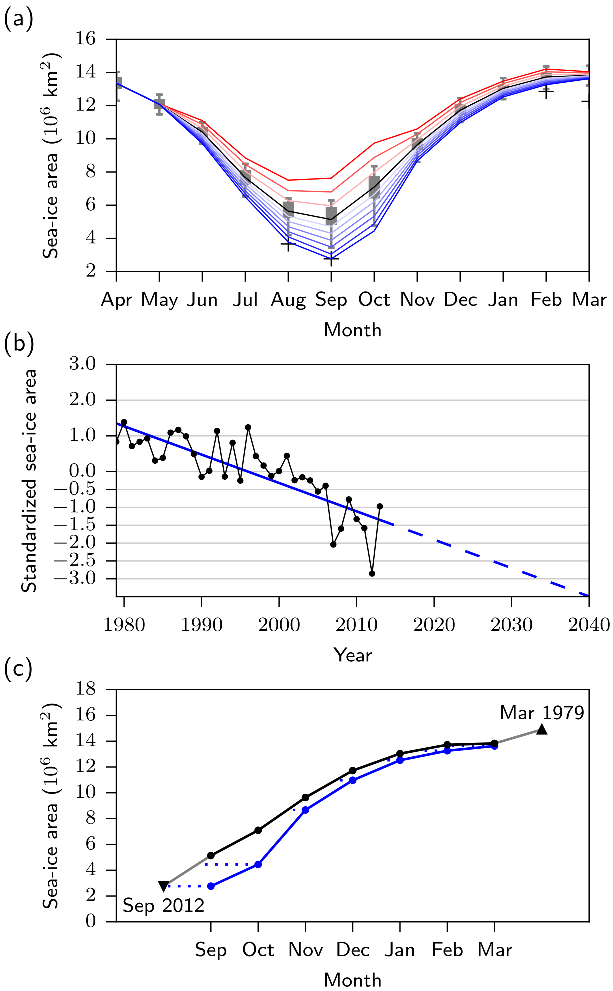

FIG. 1. (a) Seasonal cycle of Arctic sea ice area for all sea ice scenarios, ranging from $\alpha = 0$ (unperturbed control run; black line) to $\alpha = -0.5, -1, -1.5, -2, -2.5, -3$ (from light-blue to dark-blue lines) and $\alpha = 1, 2, 3$ (from light-red to dark-red lines). Gray boxes cover from the lower to upper quartile of Arctic sea ice areas in observations from 1979 to 2013, whiskers extend from the boxes to 1.5 times the interquartile range, and plus marks show observations outside the whisker range. (b) Correspondence between observed September Arctic sea ice areas (black dots) and the perturbation parameter α. The blue solid line is the linear trend over 1979–2013, and the blue dashed line is a linear extrapolation of the trend. (c) Sea ice areas during the freezing season for the control run (black line) and the -3 scenario (blue line), as in the right half of (a) from September. The blue dotted horizontal lines indicate how the sea ice concentration fields for the -3 scenario were derived by linearly interpolating between the monthly mean sea ice concentration fields in the unperturbed control scenario. The sea ice areas in the control run were extended downward and upward using the sea ice concentration fields from September 2012 and March 1979, respectively, as indicated by the downward and upward pointing triangles, which made it possible to derive sea ice concentration fields with sea ice areas outside the range of the climatological mean seasonal cycle of Arctic sea ice area.

area and SIC field.) This procedure essentially shifts the seasonal cycle of Arctic sea ice melt and growth. Figure 1c shows an example of how the SIC fields were derived for the -3 scenario during the freezing season; the November SIC field in the -3 scenario was created by linearly interpolating between the SIC fields in October and November in the control run, the December SIC field corresponds roughly to the unperturbed SIC field three weeks into November, and so on. To derive SIC fields with areas smaller or larger than the climatological monthly mean values, we incorporated the record minimum and maximum SIC fields in climatology (September 2012 and March 1979, respectively) in our interpolations, as shown by the leftmost and rightmost points in Fig. 1c. As a result, the September sea ice coverages in our simulations approach the September 2012 conditions as α gets closer to -3.

SST fields consistent with the new SIC fields were calculated by performing the same type of linear interpolation as with the SIC fields and selecting the SST field that corresponds to the same time as the selected SIC field. The SST was adjusted only in grid points where the SIC had changed compared with the climatological mean value in the unperturbed control run to account for SST changes associated with increased or reduced sea ice. Completely ice-filled grid cells were set to an SST of -1.8°C. Note that this temperature is the temperature below the sea ice and that the surface skin temperature (as modeled by CAM5) may be lower.

The SIC and SST fields were finally processed to preserve the monthly mean values after the model had interpolated the monthly boundary conditions to daily values, following the algorithm described by Taylor et al. (2000). Figure 2 shows the SIC perturbations in autumn and early winter for the 3, -1, -2, and -3 scenarios, and the corresponding SST perturbations are shown in Fig. 3. We note that the SST perturbations (Fig. 3) are generally much smaller than the surface skin temperature anomalies felt by the atmosphere (in December the maximum surface skin temperature anomaly exceeds 12.7 K in the -3 scenario compared to the control run). To summarize, our sea ice scenarios emulate one mode of interannual Arctic sea ice variability under a warming climate; scenarios with smaller α values have a smaller Arctic sea ice coverage in September, faster ice melt during the melt season, and slower growth of sea ice during the freeze season, and vice versa for scenarios with larger α values.

c. Diagnostic methods

To diagnose the model response to the varying sea ice perturbations, we examined the linear monthly

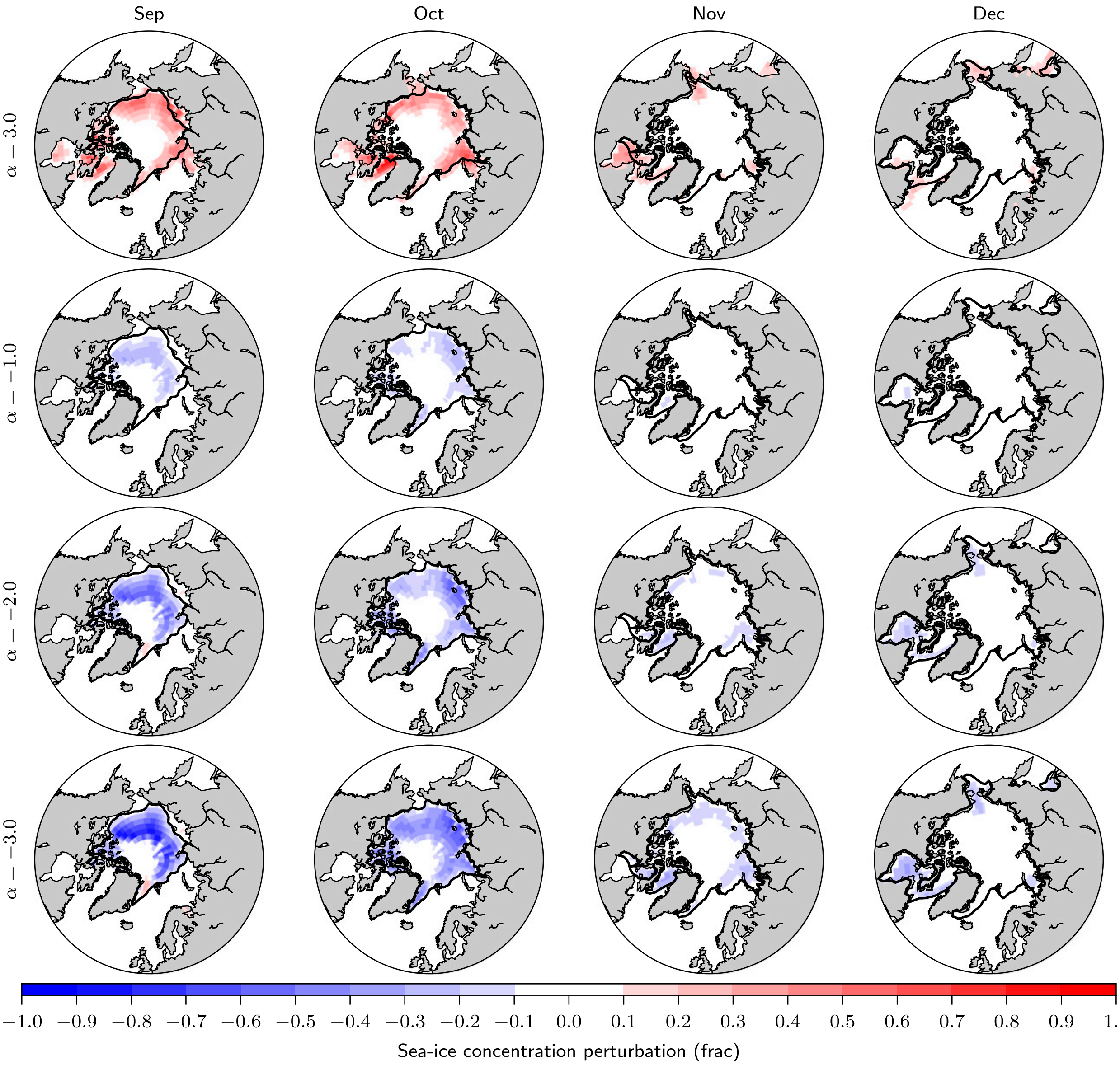

FIG. 2. Spatial patterns of the monthly mean SIC perturbations for the (top)–(bottom) 3, −1, −2, and −3 sea ice scenarios in (left)–(right) September, October, November, and December, compared with the control run (0 scenario). The thick black line shows the sea ice boundary in the control run where the SIC exceeds 15%.

mean response in different atmospheric variables, change in position and waviness of the Northern Hemisphere polar jet stream, meridional extent of large-scale Rossby waves, frequency of large-scale atmospheric circulation patterns, and occurrence of extreme cold events in different midlatitude regions.

The position of the Northern Hemisphere polar jet stream was tracked using the vertically integrated mass flux between 925 and 700 hPa and 40°–65°N latitude. We averaged the mass flux over the lower troposphere to focus on the equivalent barotropic polar jet and to exclude the variability associated with the subtropical jet, which is localized mostly in the upper troposphere. Following the method of Archer and Caldeira (2008), the latitudinal position of the jet stream was calculated for each longitude band as the mass-flux-averaged latitude. The jet stream analyses were repeated using the location of the maximum zonal wind integrated over the lower troposphere.

The waviness of the jet stream was measured for each ensemble member as the root-mean-square deviation

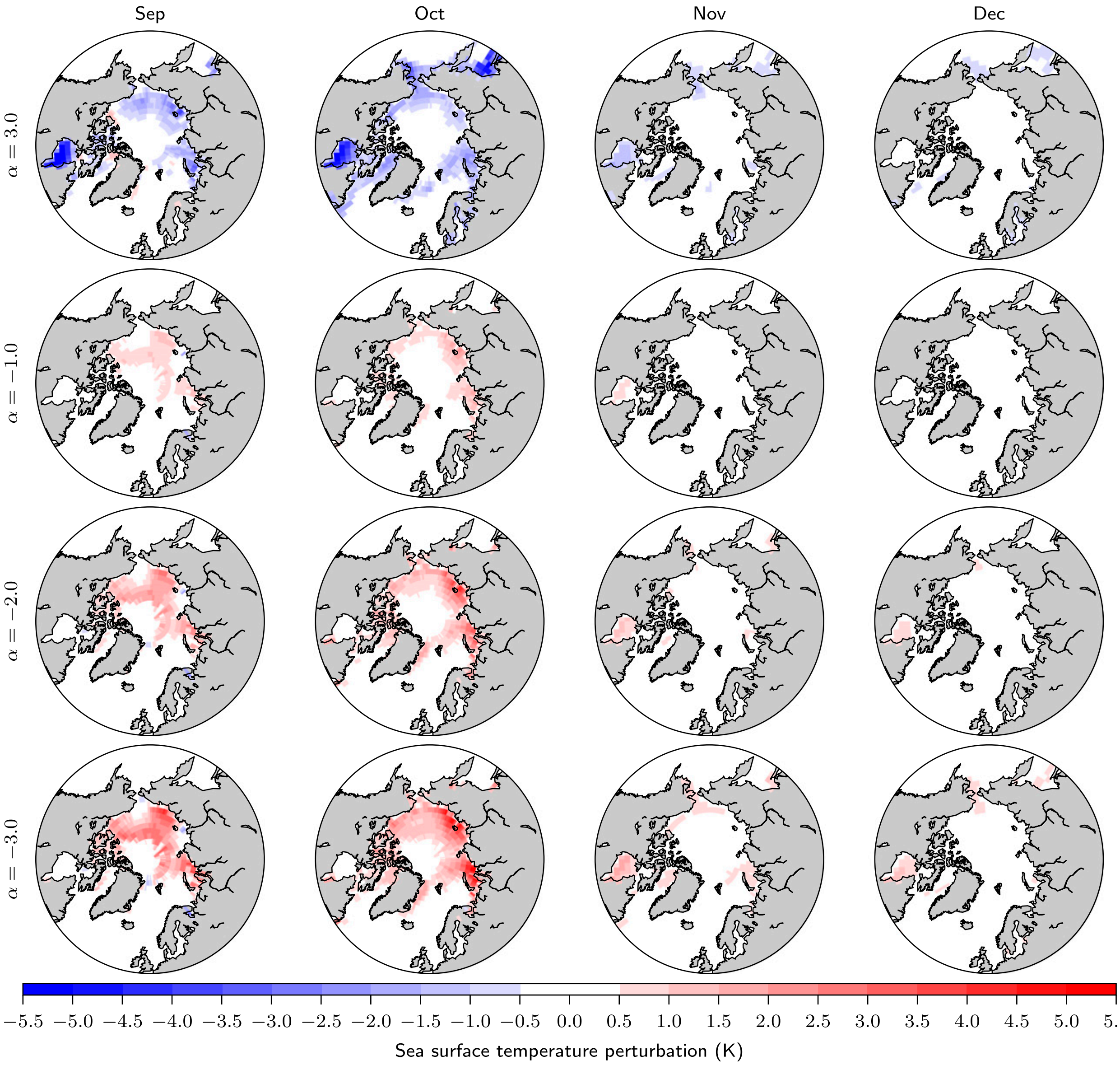

FIG. 3. Spatial patterns of the monthly mean SST perturbations associated with sea ice loss for the (top)–(bottom) 3, −1, −2, and −3 sea ice scenarios in (left)–(right) September, October, November, and December, compared with the control run (0 scenario).

(RMSD) from the zonally averaged ensemble mean latitude of the jet stream position:

$$\mathrm{RMSD}_{m,t} = \sqrt{\frac{1}{n}\sum_{i=180^\circ}^{180^\circ}(\phi_{m,t,i} - \langle\phi_{m,t}\rangle)^2},$$

where m and t are indices for ensemble member and time, respectively, and the sum over i is over all longitude bands. The latitudinal position of the jet stream is ϕ, $\langle\phi\rangle$ is the zonally averaged latitudinal position, and n is the total number of longitude bands. The RMSD was also calculated over different longitudinal sectors (Fig. 4a): AtlanticNA (130°–10°W), wAsiaEurope (10°W–110°E), and eAsiaPacific (110°E–130°W).

We further quantified the changes in the upper-level flow resulting from the prescribed sea ice perturbations by calculating the meridional extent of large-scale Rossby waves at the 500-hPa level using the wave extent metric of Barnes (2013). The wave extent is defined as the difference between the maximum and minimum latitude of a specific 500-hPa geopotential height contour. Following Barnes (2013), we calculated the wave extent using daily geopotential heights over a range of isohypses (5000–6000 m) and chose the isohypse with the maximum wave extent for each day. The daily wave

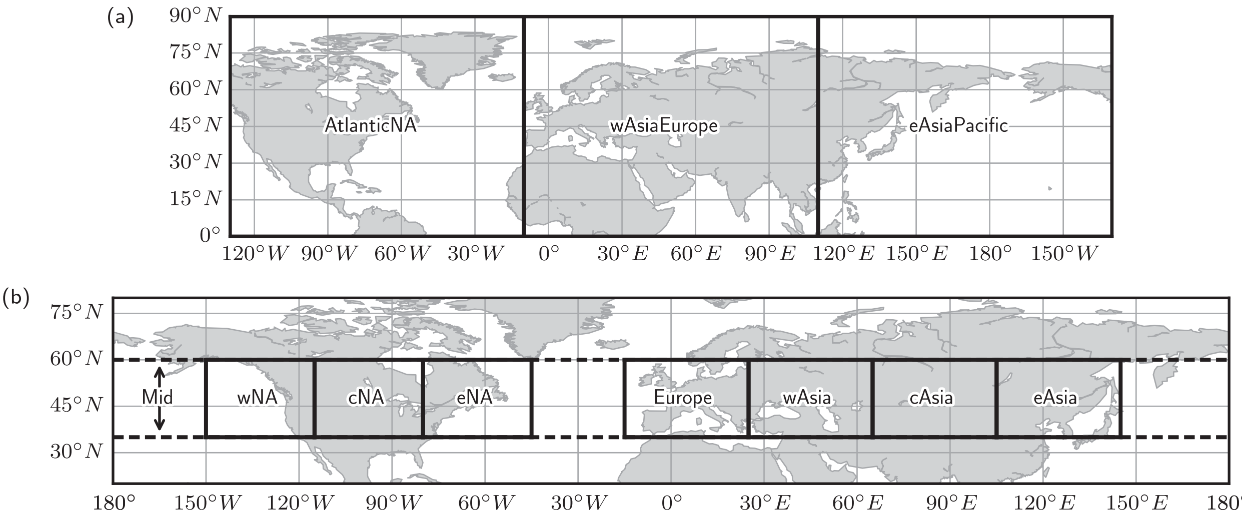

FIG. 4. Geographical regions used in (a) the jet stream and wave extent analyses and (b) the extreme cold event analysis. The regions are shown within black boxes and labeled by their abbreviated names. Dashed lines in (b) show the Mid region, which covers the land over the whole midlatitudes.

extents were then averaged over each month to obtain monthly mean wave extents. We refer to Barnes (2013) and Barnes and Polvani (2015) for more information about this wave extent metric and discussions on why it is important to use a range of isohypses instead of a single 500-hPa geopotential height contour. The wave extent analysis was carried out in the Northern Hemisphere over all longitudes and over the same longitudinal sectors as in the jet stream analysis (shown in Fig. 4a). Note that the AtlanticNA region is the same region as used by Barnes (2013) and Barnes and Polvani (2015).

To examine the impact of Arctic sea ice loss on the large-scale circulation in the following winter, we clustered daily patterns of sea level pressure anomalies northward of 30°N in December through February (DJF) and calculated the frequency of occurrence of each cluster pattern. We chose to use daily model output, rather than monthly or seasonal means as is commonly done in the literature, to better resolve the transient systems that are important for the heat and moisture transports in the Arctic climate system (Simmonds and Keay 2009). The anomalies were obtained by subtracting the seasonal cycle from each grid point, which was found by fitting a constant term and two pairs of sine and cosine terms to the control simulations.

The high-dimensional daily data were objectively clustered into nine clusters using a self-organizing map (SOM; Kohonen 1982), where each cluster represents a large number of similar circulation anomaly patterns. The SOM algorithm finds a number of representative patterns by minimizing the Euclidean distance between the representative patterns and the daily fields. Previous studies have shown that the variability of large-scale circulation patterns in the Northern Hemisphere is well described by a continuum of teleconnection patterns (Franzke and Feldstein 2005) that can be found through a self-organizing map analysis (Johnson et al. 2008).

We chose a SOM size of 3×3 clusters as a compromise between a small number of clusters and a high correlation between daily fields and their corresponding representative SOM cluster. As the average correlation of all clusters increases by less than 0.008 for each row or column that is added after reaching a size of 3×3 clusters, we conclude that 3×3 clusters are sufficient for the purpose of our study. Before the SOM training and mapping, the sea level pressure anomalies were weighted by the square root of the cosine of latitude to account for the increasing grid point density at higher latitudes and were unweighted again before the clusters were plotted.

To examine the frequency of extreme cold events in the midlatitudes, we divided the midlatitude continents into eight regions, the same regions as used in Screen and Simmonds (2014) (Fig. 4b): all midlatitudes (Mid; 35°–60°N, all longitudes), western North America (wNA; 35°–60°N, 150°–115°W), central North America (cNA; 35°–60°N, 115°–80°W), eastern North America (eNA; 35°–60°N, 80°–45°W), Europe (35°–60°N, 15°W–25°E), western Asia (wAsia; 35°–60°N, 25°–65°E), central Asia (cAsia; 35°–60°N, 65°–105°E), and Eastern Asia (eAsia; 35°–60°N, 105°–145°E). For each region we calculated a temperature index, obtained as the area-averaged 2-m temperature over land. The temperature indices were smoothed using a 5-day moving average to filter out temperature variations on time scales shorter than the synoptic scale. An extreme cold event was defined as an event when the temperature index fell below the 2.5th percentile of all 550 ensemble members for a particular day during winter (DJF).

When testing the significance of the results from the different diagnostics, we typically compared the results from one sea ice scenario with the whole sample of 550 ensemble members from all 10 sea ice scenarios, rather than testing if the results are statistically different from only the control run. This method of significance testing provided more robust results because less emphasis was placed on the unperturbed control scenario; thus, other than deriving the initial conditions from the control run, the 0 scenario was treated the same as the other nine perturbed sea ice scenarios. To make sure that this test of significance was robust, we repeated the significance testing by comparing the results from one sea ice scenario with the control scenario, as well as comparing with scenarios with a whole number for α (to avoid biases due to the unbalanced number of perturbed scenarios above and below 0) and all scenarios except the one that is currently being compared, with no change to the overall conclusions.

3. Results

a. Correlation with atmospheric variables

We quantified the strength of the linear relationship between reduced Arctic sea ice and the atmospheric response by correlating monthly mean model output from all 550 ensemble members with the sign-reversed sea ice area perturbations α corresponding to each ensemble member. The sign of the perturbations was reversed to show the changes associated with decreasing sea ice area. This ensemble correlation analysis is analogous to regressing atmospheric variables onto the sea ice area anomalies, which is commonly done in observational studies, the difference being that correlation coefficients are normalized to 1 and unitless. Correlation coefficients further away from 0 indicate stronger linear relationships between the atmospheric response and the forced sea ice anomalies.

We find the strongest linear response to reduced sea ice in autumn over and in the immediate vicinity of regions of sea ice retreat, with significantly increased sensible and latent heat fluxes (not shown), which led to an increased 2-m air temperature in a large part of the Arctic (Figs. 5a–c), consistent with results from previous studies (e.g., Alexander et al. 2004; Porter et al. 2012). Correlations with 2-m temperature are strongest in September when the sea ice variations are largest. The spatial pattern of positive correlation coefficients expands in area in October to encompass most of the Arctic region and the northernmost part of the Northern Hemisphere continents. In November the correlations become weaker and are mostly found over the ocean.

A similar but weaker response is seen in winter (Figs. 5d–f), partly owing to the persistence of the forced sea ice anomalies. Some significant correlation coefficients ($p < 0.05$) are now found farther to the south where the largest SIC anomalies are located (most of the Arctic is sea ice covered at this time). In particular, we see a large warming associated with sea ice loss in the vicinity of the Barents and Kara Seas, the Sea of Okhotsk, Hudson Bay, and the Chukchi and Bering Seas. The remote linear response in the midlatitudes, however, is weak and generally statistically insignificant, similar to the findings of previous studies (see, e.g., Screen et al. 2014). Figure 5f shows cooling in Canada in February associated with Arctic sea ice loss, but the linear relationship explains less than 4% of the 2-m temperature variance. The regions with significant correlation coefficients are otherwise still largely located over the ocean. The largest surface warming exceeds 10 K in December in the ensemble mean of the −3 sea ice scenario compared with the 0 scenario, with a difference of around 1 K for every 0.5 change in α value in the scenarios with a negative sea ice perturbation.

Correlations with sea level pressure (Fig. 6) are much smaller than those with 2-m temperature (Fig. 5) and mostly reflect a thermodynamic response to surface warming. The strongest linear relationships between sea ice loss and sea level pressure are a lower-than-usual pressure in the Arctic basin in October (Fig. 6b) and low pressure centered over Hudson Bay in December (Fig. 6d). The ensemble mean responses in sea level pressure compared with the mean of all sea ice scenarios are generally statistically insignificance for most sea ice scenarios except for the −2 scenario, which shows a weakening of the Icelandic low and Azores high in winter (DJF), resembling the negative phase of the AO in the North Atlantic sector (not shown). Similarly to the weak linear response in sea level pressure, the correlation with geopotential heights is weak and mostly insignificant, with correlation coefficients smaller than 0.2 in magnitude, most of which reflect the surface warming and exhibit an equivalent barotropic structure that extends into the stratosphere (not shown). Restricting the correlation analysis to limited sets of sea ice scenarios (small perturbations within ± 1 for α, only positive perturbations, and only negative perturbations) resulted in correlation coefficients of similar magnitude for sea

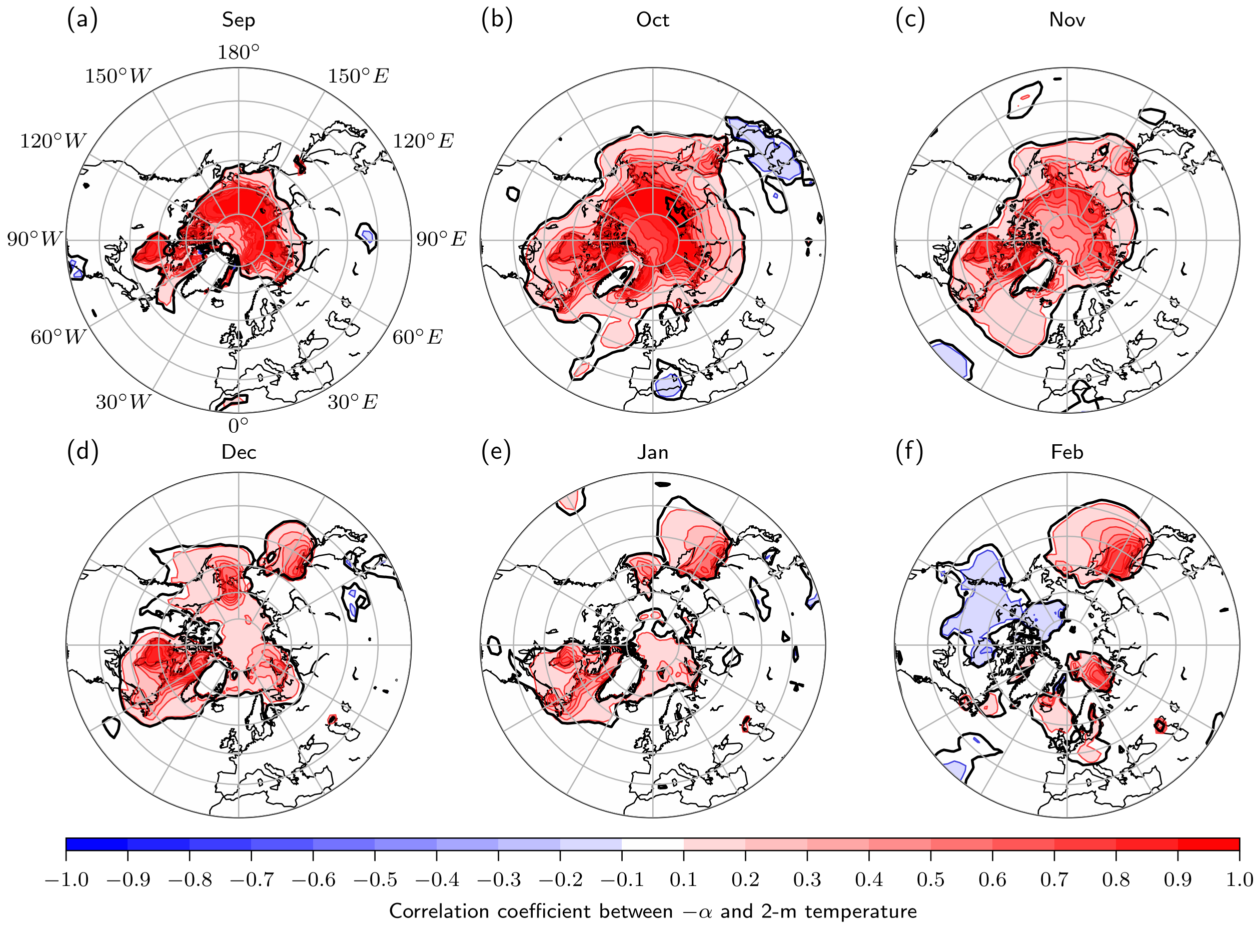

FIG. 5. Correlation coefficients between sign-reversed α and 2-m temperature in (a) September, (b) October, (c) November, (d) December, (e) January, and (f) February. Black contours indicate correlation coefficients that exceed the 95% confidence level.

level pressure, geopotential heights, and 2-m temperature in the midlatitudes. These results show that the linear relationship between Arctic sea ice loss and midlatitude weather patterns is weak, suggesting that the remote atmospheric response is small compared with the internal variability, or highly nonlinear with respect to the sea ice area anomalies.

b. Jet stream and upper-level wave extent

The warming of the Arctic and weakening of the meridional temperature gradient scale approximately linearly with the sea ice reductions (Fig. 5). One might expect the resulting decrease in the horizontal temperature gradient to alter the position of the Northern Hemisphere polar jet stream based on observations from previous studies (Francis and Vavrus 2012, 2015). In our simulations, however, the ensemble mean differences in the monthly mean jet stream position between different sea ice scenarios are less than 1° in the latitudinal direction and generally much smaller than the ensemble spread (Fig. 7). There is evidence of a slight southward shift of the jet stream in the −2 scenario (Fig. 7b), but there is no sign of a meridionally elongated jet stream associated with Arctic warming.

Figure 8 shows the ensemble mean shifts of the winter jet stream in the different sea ice scenarios, which generally fall within the range of internal variability. The southward shift of the jet stream in December for the −2 scenario is seen again in Fig. 8h. We also see that the mean shifts in the position of the polar jet stream are very different across sea ice scenarios and there is no common robust response that can be found in two scenarios or more. In the −3 scenario, which has the largest Arctic warming out of all sea ice scenarios, the ensemble mean differences in jet stream position are minuscule and no more significant than what would be expected from random noise.

It is conceivable that the jet stream amplitude increased in individual ensemble members and that the jet stream shifts occurred at different locations in such a way the changes canceled out in the ensemble mean. To account for this possibility, we quantified the monthly

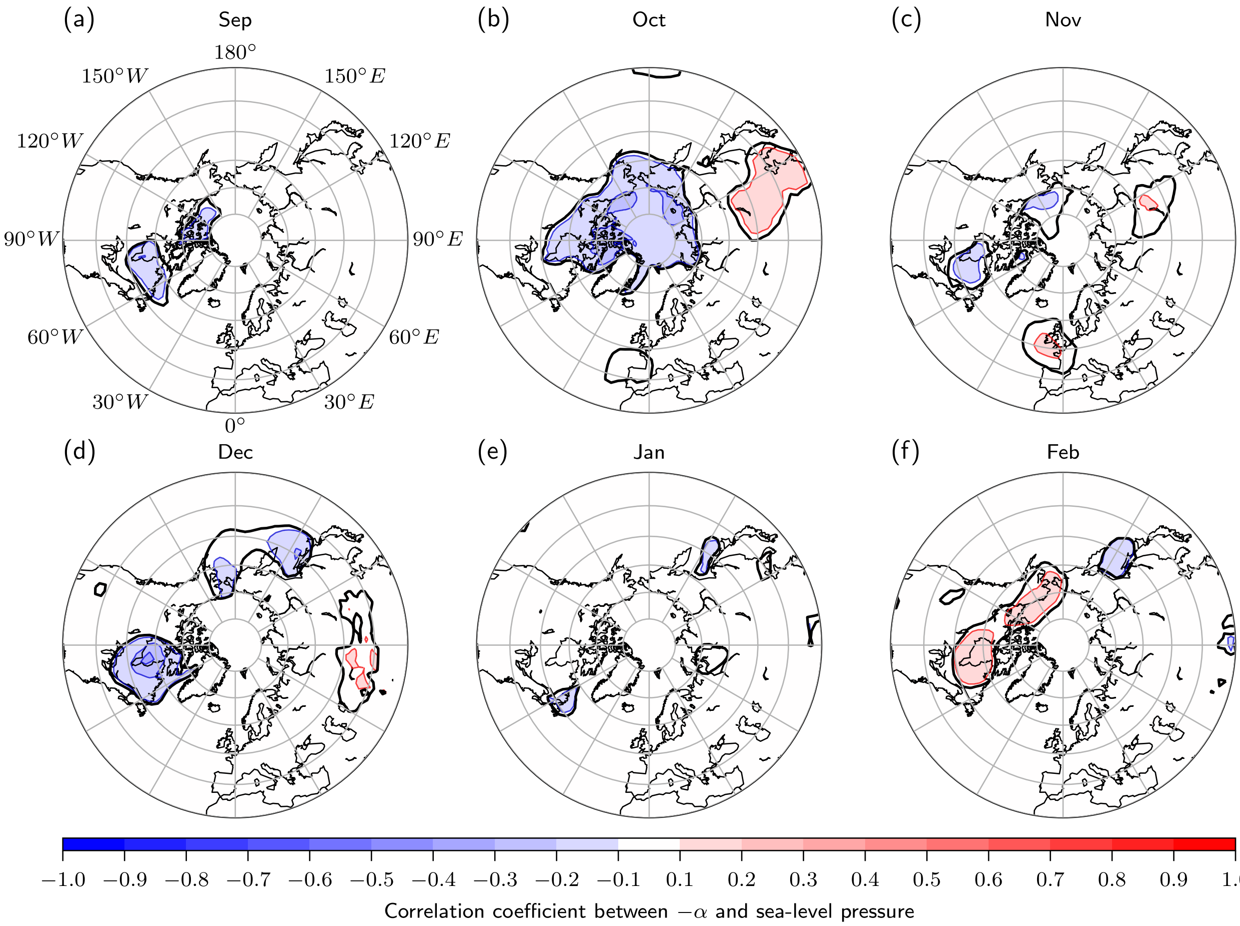

FIG. 6. As in Fig. 5, but for the correlation coefficients between sign-reversed α and sea level pressure.

mean waviness of the jet stream for each individual ensemble member by calculating the RMSD from the zonally averaged jet stream position (see section 2). A larger RMSD indicates a larger wave amplitude (i.e., a wavier jet stream), whereas a smaller deviation corresponds to a more zonal flow. Figure 9a shows the ensemble mean RMSD anomaly for each sea ice scenario and the ensemble spread (one standard deviation). There are small variations in RMSD between scenarios, but these variations are again dwarfed by the large intrinsic variations within individual scenarios. The linear trends in RMSD are close to zero or slightly negative (i.e., decreasing jet stream amplitude with decreasing sea ice areas). Thus, our results do not show evidence of an unusually elongated jet stream associated with Arctic sea ice loss on a monthly time scale.

The jet stream analyses were repeated over different longitudinal sectors, which yielded similar results. We note that the metric we used to determine the position of the jet stream (i.e., the average of the latitude weighted by the vertically integrated mass flux) is rather conservative, in the sense that a change in the upper-level mass flux leads to a rather small change in the position. Because of the definition of the metric, the lines in Fig. 7 tend to not exactly track values of maximum mass flux. We also tried slightly modified metrics, such as increasing the weights of higher values of mass flux or following the maximum zonal wind at each longitude band. These modifications led to larger differences between sea ice scenarios but also much larger ensemble spread within the scenarios and ultimately did not change the conclusions from the above analyses. In conclusion, our simulations suggest that any potential links between reduced Arctic sea ice as implemented here and the polar jet stream are more complex than described by a simple linear relationship.

We further quantified the waviness of the upper-level flow by calculating the maximum meridional extent of the 500-hPa isohypses. Figure 9b shows the ensemble mean anomaly and ensemble spread (one standard deviation) of this wave extent metric for the different sea ice scenarios. As with the jet stream analysis, the intrinsic variability of the wave extent within each sea ice scenario overshadows the small differences between the ensemble means of different scenarios. Consequently,

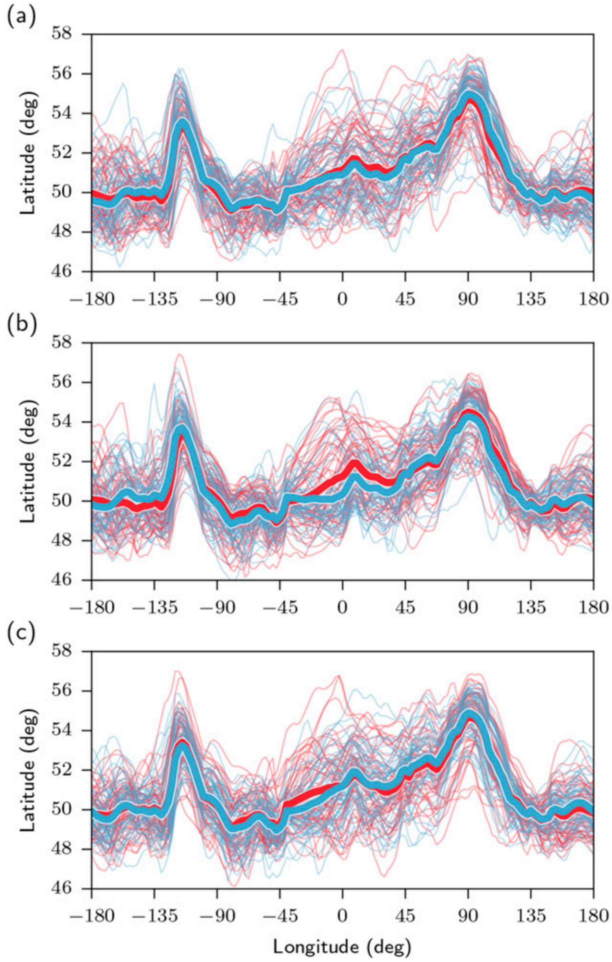

FIG. 7. Position of the Northern Hemisphere polar jet stream in December with increased (red) and decreased (blue) Arctic sea ice coverage for the sea ice scenarios (a) 1 and −1, (b) 2 and −2, and (c) 3 and −3. Thin lines show the jet stream position of individual ensemble members and thick lines represent the ensemble mean position.

we conclude that our simulations do not show a robust link between Arctic warming associated with sea ice loss and increased amplitude of upper-level waves.

c. Large-scale circulation patterns in winter

To quantify the changes in daily large-scale circulation patterns during winter resulting from Arctic sea ice loss, we clustered the sea level pressure anomaly patterns into nine clusters (C1–C9) using a SOM, which are shown in Fig. 10. The C1 and C9 patterns show some resemblance with the positive and negative phase of the AO, respectively, but they are more regional in structure compared with the annular structure of the AO, with a weaker action center over the Azores and an eastward shift of the center over the Arctic. C9 is similar to the (1, 1) node of the SOM in the observational study of Johnson et al. (2008). The action center over the Arctic closely resembles the leading mode of variability of daily sea level pressure anomalies in the model output (found as the first empirical orthogonal function; not shown). Although C1 and C9 do not match exactly the classical pattern of the AO, a sea level pressure pattern that projects strongly onto the AO will be classified as one of these SOM clusters, so we will refer to these patterns as the positive and negative AO-like patterns, respectively. C3 and C7 mainly reflect the sea level pressure variability associated with the Pacific–North American pattern. The remaining clusters describe the transition between these dominant teleconnection patterns.

Figure 11 shows the frequency of occurrence of days falling into each circulation-anomaly cluster for each sea ice scenario. There is a statistically significant increase in the frequency of the negative AO-like pattern (C9) in three scenarios with reduced Arctic sea ice: −0.5, −2, and −2.5. For the −2 scenario, this increase is accompanied by a decreased frequency of the positive AO-like pattern (C1). We note that the negative AO signal extends up into the stratosphere in some scenarios, manifested as a weakening of the stratospheric polar vortex, which is especially strong in the −2 scenario and to some extent the −0.5 scenario (not shown). Most of the other cluster frequency changes in Fig. 11 are small and not clearly distinguished from random variations.

The shift toward a more frequent negative phase of the AO is consistent with findings from other studies (Deser et al. 2010; Hopsch et al. 2012; Liu et al. 2012; Peings and Magnusdottir 2014; Screen et al. 2013); however, our large ensemble of simulations with varying sea ice forcing reveals that this response is significant in only three out of our six scenarios with reduced Arctic sea ice, with a highly statistically significant increase in the −0.5 and −2 scenarios and a statistically significant increase in the −2.5 scenario (all at the 95% confidence level). In the sea ice scenario with most severe sea ice loss (−3), on the other hand, the frequency of the negative AO-like circulation pattern (C9) is significantly decreased (Fig. 10). Furthermore, two scenarios (−1.5 and −3) with decreased Arctic sea ice coverage show an increase in the frequency of the positive AO-like circulation pattern (C1), although this increase is only marginally significant. From the SOM analysis we conclude that the tendency for a negative AO pattern as a result of declining Arctic sea ice is nonrobust and only occurs under certain conditions, which could depend on the state of internal variability of the climate system.

d. Extreme cold winter events

Next we focused on the influence of Arctic sea ice loss on extreme cold winter days over the midlatitude continents.

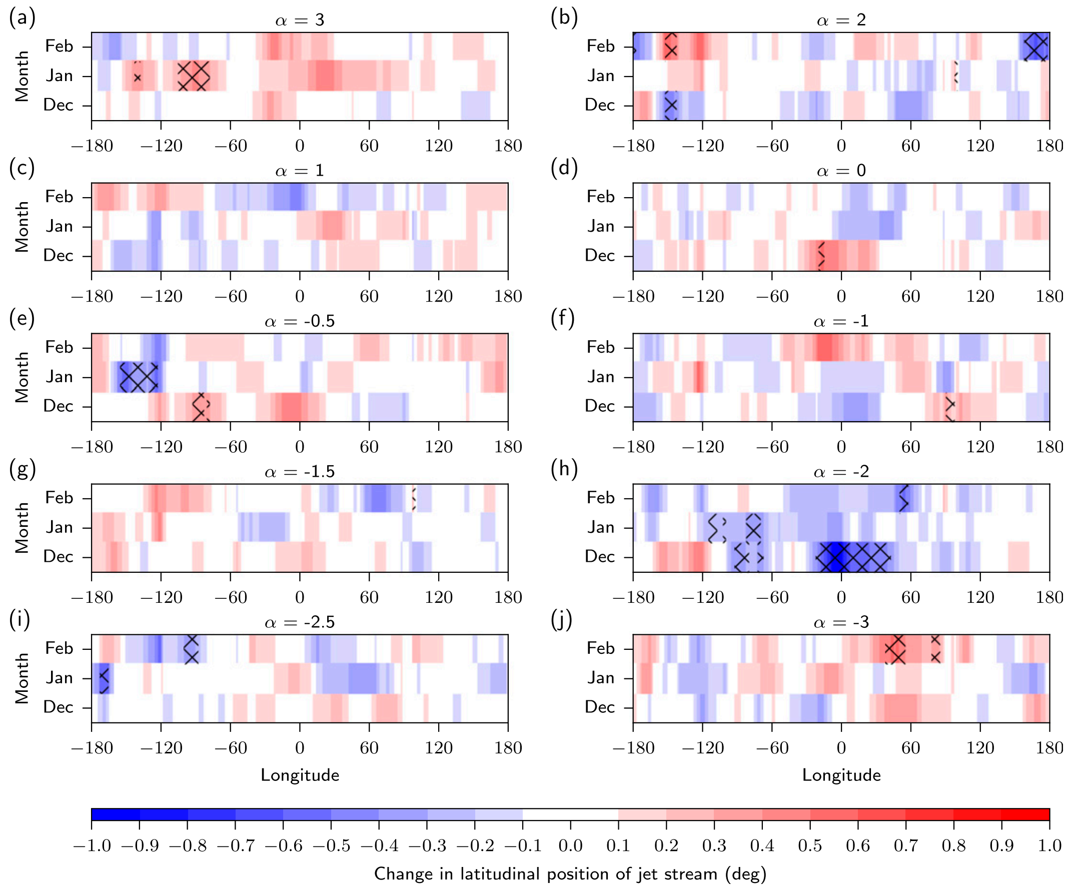

FIG. 8. Deviations in the ensemble mean jet stream position for the sea ice scenarios (a) 3, (b) 2, (c) 1, (d) 0, (e) −0.5, (f) −1, (g) −1.5, (h) −2, (i) −2.5, and (j) −3. The deviations were obtained by subtracting the average jet stream position of all scenarios from the ensemble mean of a specific scenario. Cross hatching indicates significant differences from the mean position according to a Student's t test ($p < 0.05$).

The midlatitude continents were divided into eight regions (Fig. 4b), and for each region we calculated the frequency of extreme cold winter events (i.e., days in DJF when the daily area-averaged 2-m temperature fell below the 2.5th percentile; see section 2), shown in Figs. 12a–h. We find a statistically significant increase in extreme cold events in eastern Asia (Fig. 12h) in the −0.5, −2, and −2.5 scenarios, the same scenarios that experienced a more frequent negative AO-like (C9) circulation pattern. In central Asia (Fig. 12g), extreme cold events are most common in the unperturbed scenario and those with moderately reduced sea ice but are relatively rare for more extensive or less extensive sea ice. Extreme cold events in central and eastern Asia typically occur following periods when the circulation pattern best matches the C9 negative AO pattern (not shown). Eastern Asia is likely more sensitive to the increased frequency of C9 because of the position of the positive action center over the Arctic, which could lead to anomalous northeasterly winds and increased advection of cold Arctic air into this region.

Conversely, in some regions there is a statistically significant decrease in the frequency of extreme cold events associated with Arctic sea ice loss. This is most notable in eastern North America (Fig. 12d), where the frequency of cold events declines almost linearly with decreasing sea ice coverage. This contrast between increased frequency of extreme cold events in parts of Asia and decreased frequency in eastern North America agrees with the results of other recent studies (Mori et al. 2014; Screen et al. 2015a). For the −3 scenario, which used the 2012 record-low sea ice in September and may represent the mean sea ice state in a few decades if the current trend continues (Fig. 1b), we find that the frequency of extreme cold events is either within expected climatological values or significantly decreased in all regions. Our finding of a reduction in the number of extreme cold events in the scenario with largest Arctic warming is consistent with the expectation of decreased synoptic surface temperature variance in the midlatitudes due to Arctic amplification (Schneider et al. 2015; Screen 2014; Sun et al. 2015).

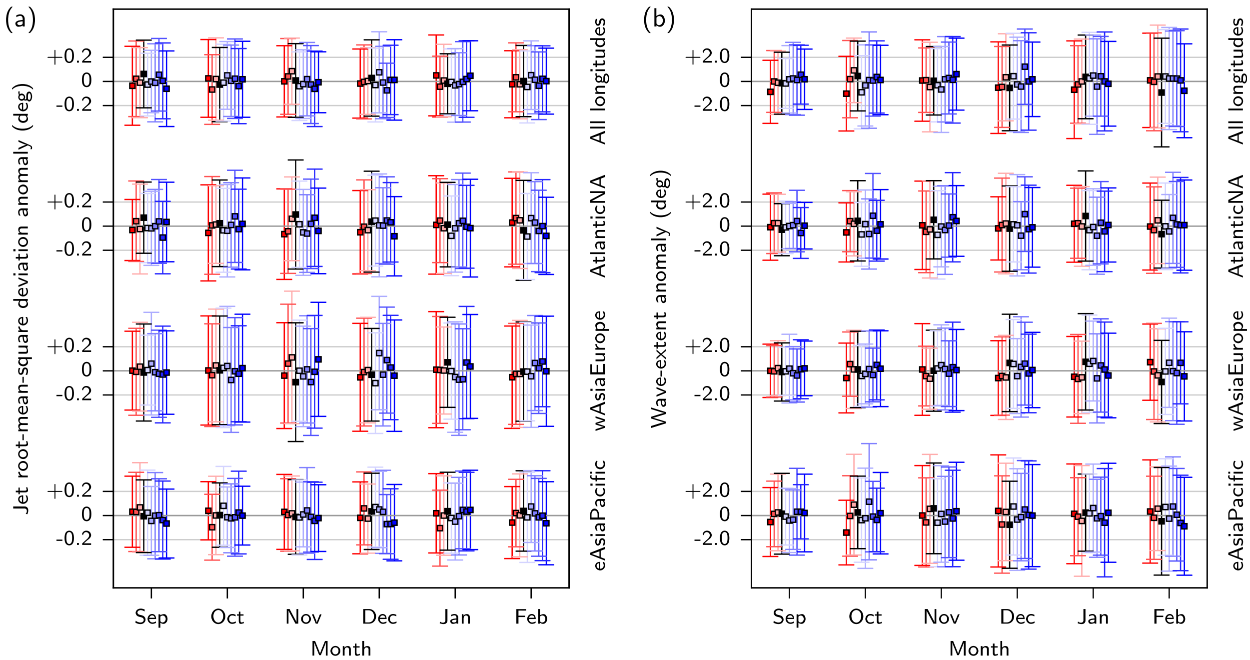

FIG. 9. (a) Changes in waviness of the Northern Hemisphere polar jet stream compared with the mean of all sea ice scenarios. A positive RMSD anomaly indicates a more meridionally elongated jet stream. Squares show the ensemble mean RMSD anomaly and error bars represent one ensemble standard deviation from the mean. The colors correspond to the following sea ice scenarios for each month–region pair: (from left to right) $\alpha = 3, 2, 1$ (dark red–light red); $\alpha = 0$ (black); and $\alpha = -0.5, -1, -1.5, -2, -2.5, -3$ (light blue–dark blue). (b) As in (a), but for the maximum meridional extent of the 500-hPa isohypses.

Previous studies have highlighted the small signal-to-noise ratio of the remote atmospheric response to Arctic sea ice loss (Screen et al. 2014) and the need for large ensembles to detect the remote response (Alexander et al. 2004; Mori et al. 2014). In the extreme cold events analysis we used all 550 ensemble members to test the null hypothesis that the samples from the different sea ice scenarios were drawn from the same population. If the null hypothesis is true, we would expect about 95% of the frequencies in Fig. 12 to fall within the gray shading. An alternative way of testing the significance is to examine the linear trend in the frequency of extreme cold events between sea ice scenarios. To this end, we fitted a generalized linear model (with Poisson error distribution and identity link function) to the frequencies in Fig. 12. We repeated this regression analysis over three sets of sea ice scenarios: first half (3, 2, 1, 0, and −0.5), second half (−1, −1.5, −2, −2.5, and −3), and all sea ice scenarios (from 3 to −3). The trends and associated p values are summarized in Table 1. Using this approach, we find a statistically significant but generally weak linear trend in the frequency of extreme cold events over all sea ice scenarios in more than half of the regions. The trends in the first half and the second half are of opposite sign in half of the regions (Mid, wNA, cAsia, and eAsia), resulting in a weaker and sometimes insignificant linear trend over all sea ice scenarios, which again reveals the nonrobustness of the midlatitude response to Arctic sea ice loss. The trends in extreme cold events in eastern Asia between the control run (0 scenario) and the −0.5, −2, and −2.5 scenarios are highly significant (p values on the order of 10^{-4} or smaller), whereas the linear trend between the control run and the rest of the sea ice scenarios is insignificant ($p > 0.05$) for all cases except the −1.5 scenario, confirming that the statistically significant changes in extreme cold winter events shown in Fig. 12 are most likely not due to random variations between ensemble members.

4. Discussion and conclusions

Here we have performed a series of model experiments in CAM5 where we systematically perturbed the sea ice cover in the Arctic region. First we perturbed the climatological mean seasonal cycle of Arctic sea ice area, starting by increasing or decreasing the September sea ice area by a number of climatological standard deviations and then adjusting the sea ice areas in the other months based on the persistence of sea ice area anomalies in observations. Next we found unique spatial patterns of SIC from the unperturbed control run that correspond to the new sea ice areas in the perturbed

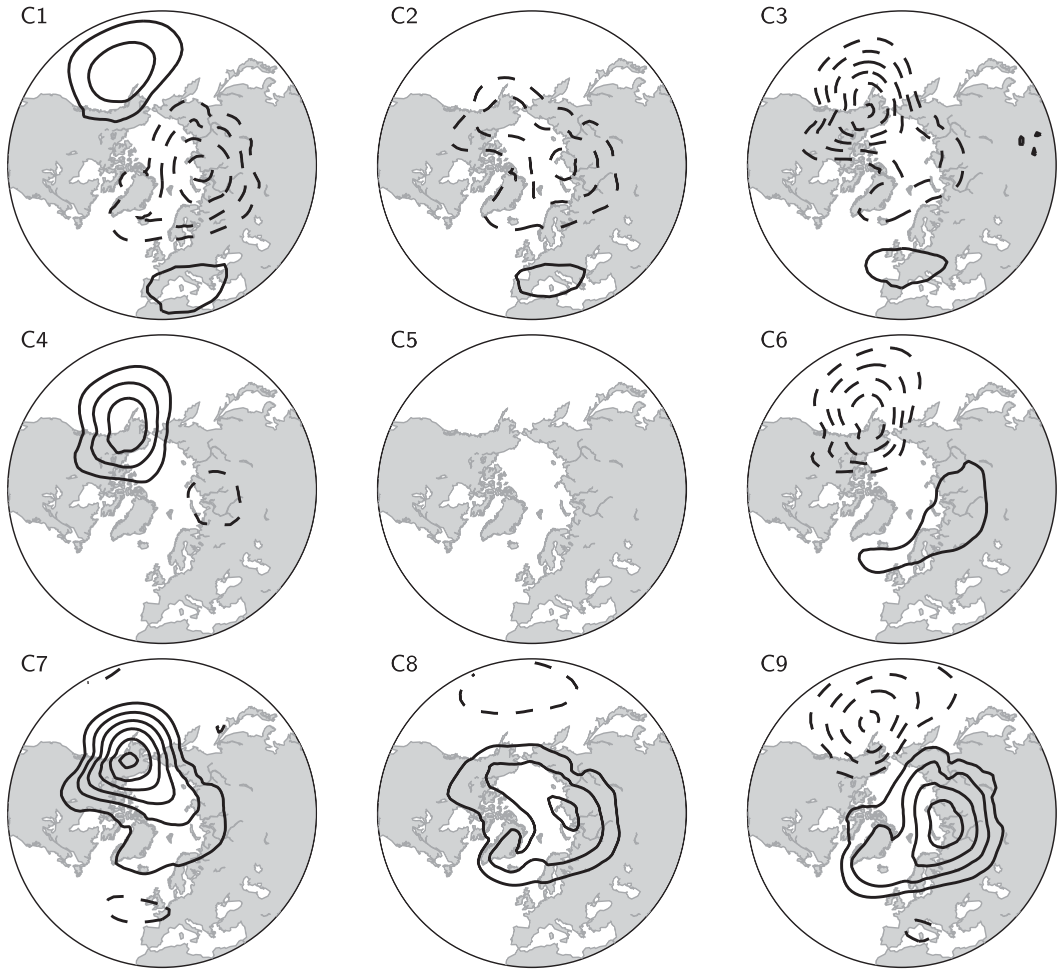

FIG. 10. Daily atmospheric circulation patterns of sea level pressure anomalies in winter (DJF) separated into nine clusters (C1–C9) through a SOM analysis. The sea level pressure anomalies are contoured every 2 hPa with the zero contour omitted, positive contours are shown with solid lines, and negative contours are shown with dashed lines.

seasonal cycle. The SICs in autumn approach the record minimum September 2012 conditions in sea ice scenarios with more severe sea ice loss. In short, we varied both the magnitude and spatial pattern of the sea ice forcing by shifting the seasonal cycle of Arctic sea ice area, which provided a natural and physically consistent emulation of a gradual sea ice decline in a warming climate.

By simulating the atmospheric response to 10 sea ice scenarios using a total of 550 ensemble members, our large-ensemble study extends the findings from previous studies that have indicated that the midlatitude response to reduced Arctic sea ice is dominated by the intrinsic atmospheric variability (e.g., Mori et al. 2014; Screen et al. 2014). Our simulations show that sea ice scenarios with 55 ensemble members can yield statistically significant signals in the midlatitudes as an atmospheric response to prescribed Arctic sea ice loss, which is especially evident in our −2 scenario, including a more frequent negative AO-like circulation pattern and increased occurrence of extreme cold winter days in eastern Asia. However, although the local response in, for example, surface temperatures (amplified warming in the Arctic) is strongly linear with respect to the Arctic sea ice loss, the link between the remote atmospheric response and sea ice variability in the Arctic is more complex than described by a direct linear relationship and is remarkably nonrobust with respect to the sea ice reductions. This nonrobust behavior of the remote response shows that disparate modeling results are not necessarily caused by differences in model setup, such as the choice of model, horizontal and vertical resolution, treatment of SST, etc., but can arise simply because of slight differences in the sea ice forcing or atmospheric conditions.

The findings of this study also have implications for the observed links between declining Arctic sea ice and

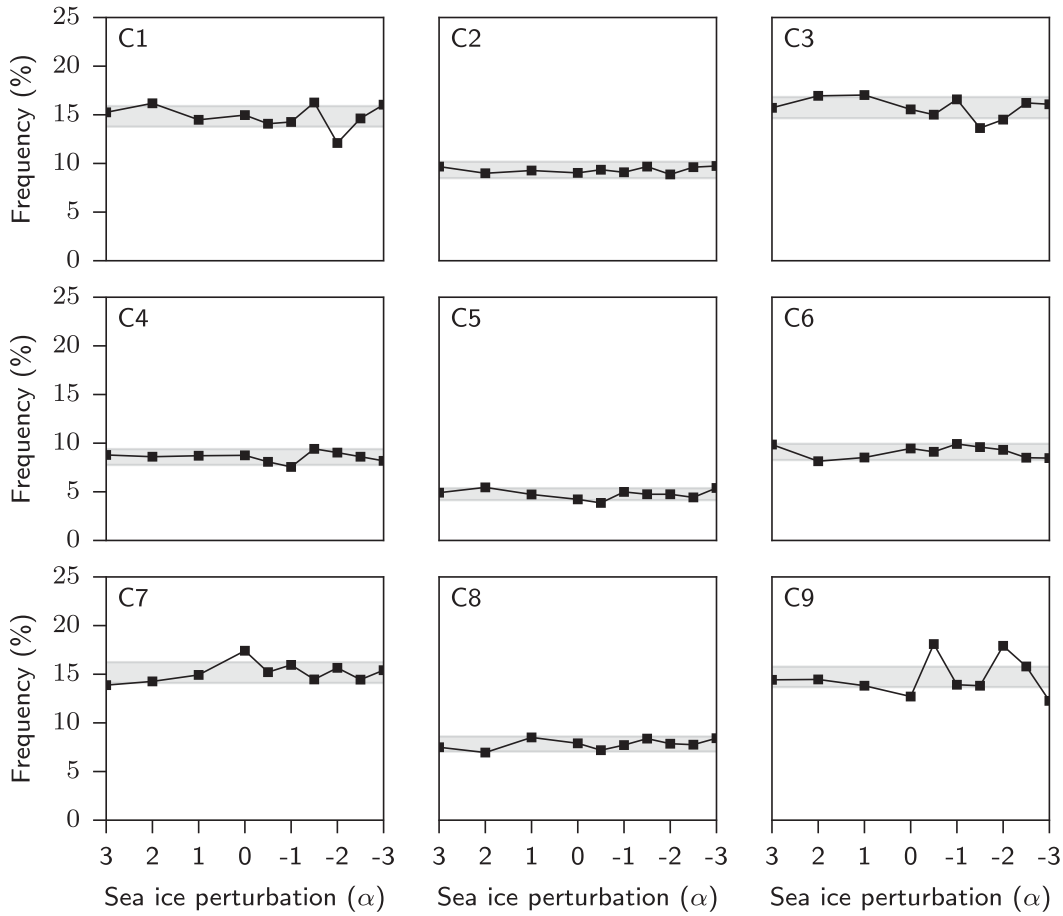

FIG. 11. Frequency of daily atmospheric circulation clusters in Fig. 10 for each sea ice scenario during winter (DJF). Frequencies outside the gray shading are significantly different from random variations according to a binomial test ($p < 0.05$).

changes in midlatitude weather patterns. In our experiments we forced ensemble members within the same scenario with an identical seasonal cycle of sea ice area, and the sea ice in the Arctic was perturbed gradually through linear methods, resulting in monotonically decreasing sea ice areas in most Arctic regions with decreasing values of the α perturbation parameter. Despite these simplifications, we find that the simulated midlatitude atmospheric response is not robust with respect to the sea ice perturbations, and linearity is generally not a valid assumption. In observations there are many factors that introduce additional noise, including other internal and external forcings that may dominate over the sea ice forcing, varying modes of spatial and temporal variability of Arctic sea ice in different years, and complex interactions and feedbacks between sea ice, the ocean, and the atmosphere. Given the increased complexity of the real climate system, it is not likely that the atmospheric response to the present Arctic sea ice loss behaves in a more robust manner in observations.

In this study we focused on one mode of Arctic sea ice variability, primarily in the September sea ice cover but with persistence of the September sea ice anomalies that prevail into the winter months, resulting in sea ice area perturbations that are directly comparable and generally encompass the range of observed sea ice area anomalies in autumn and winter. As a consequence of the persistence of sea ice area anomalies and the way we perturbed both the magnitude and spatial pattern of SICs, our sea ice forcings include sea ice perturbations during winter in regions that have been pointed out to play a key role for the wintertime atmospheric response, such as the Barents and Kara Seas (Kim et al. 2014; Petoukhov and Semenov 2010; Woollings et al. 2014) and the Sea of Okhotsk (Honda et al. 1999; Peings and Magnusdottir 2014). However, we have not considered different modes of spatial variations in the SIC field or wintertime SIC variability that is independent from the autumn variability. There are indications that sea ice loss in different Arctic regions could have opposing

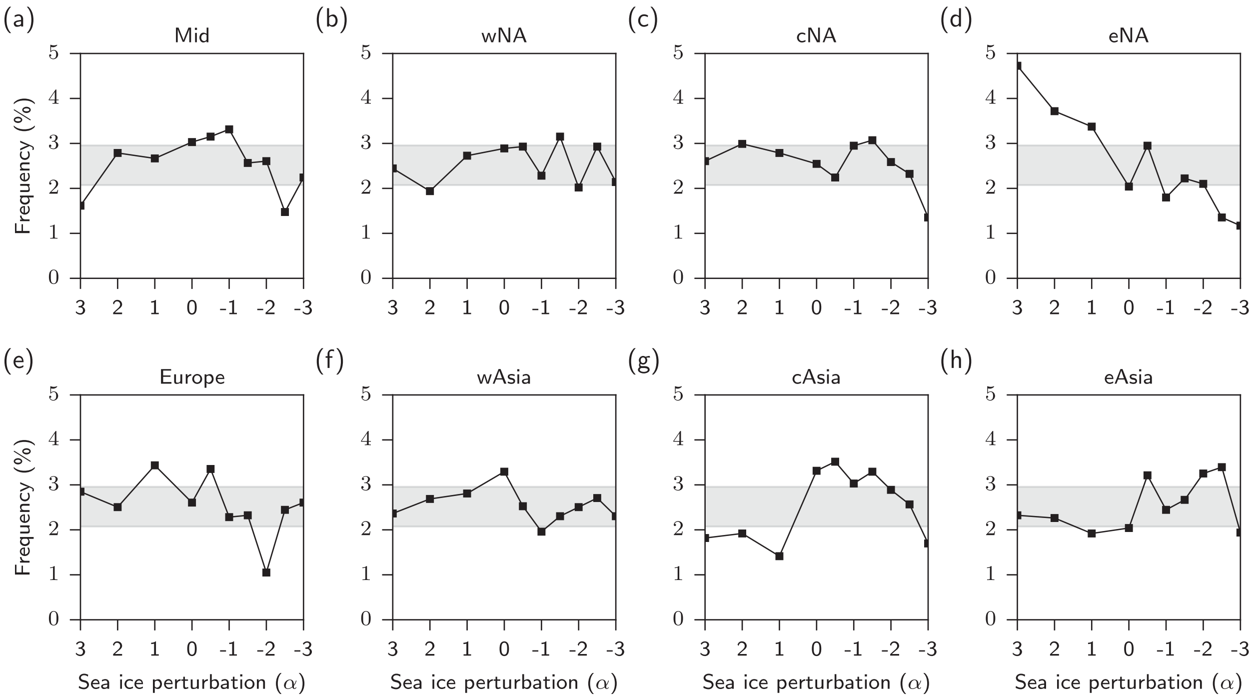

FIG. 12. Frequency of extreme cold winter days (DJF) for each sea ice scenario in regions (a) Mid, (b) wNA, (c) cNA, (d) eNA, (e) Europe, (f) wAsia, (g) cAsia, and (h) eAsia. Frequencies outside the gray shading are significantly different from random variations according to a binomial test ($p < 0.05$).

effects on the large-scale circulation (e.g., Sun et al. 2015); therefore, we may underestimate the remote atmospheric response by not accounting for different regional variations of Arctic sea ice loss. Other factors that may lead to a weaker atmospheric response in our simulations compared with the real climate system include the use of prescribed SSTs instead of an interactive ocean, which could play a crucial role especially for the long-term equilibrium response (Deser et al. 2015); not high enough model resolution to simulate some important atmospheric features such as more realistic blocking patterns (Berckmans et al. 2013; Jung et al. 2012); constant sea ice thickness (Gerdes 2006); and the neglect of forcings that originate from outside the Arctic region, such as the teleconnection pattern with a source in the North Atlantic region of the Gulf Stream that could explain some of the links between reduced sea ice in the Barents Sea and cold Eurasian winters (Simmonds and Govekar 2014). It is possible that a stronger sea ice forcing such as the projected Arctic sea ice loss for the end of the twenty-first century could result in more robust responses in some midlatitude weather patterns (e.g., Screen et al. 2015a), but on the other hand, a larger sea ice loss does not

TABLE 1. Linear trends in frequency of extreme cold events during winter (DJF) in the midlatitude regions shown in Fig. 4b. The trends were obtained from a generalized linear model with Poisson error distribution and identity link function and are expressed in units of percentage points per -1α, where α is the sea ice perturbation. We repeated the linear regression analysis over three sets of sea ice scenarios: first half (3, 2, 1, 0, and −0.5), second half (−1, −1.5, −2, −2.5, and −3), and all sea ice scenarios (from 3 to −3). Trends that are significant at the 95% confidence level and corresponding p values are shown in boldface.

	Sea ice scenarios from 3 to −0.5		Sea ice scenarios from −1 to −3		All sea ice scenarios	
Region	Trend	p value	Trend	p value	Trend	p value
Mid	**0.36**	**2.0×10^{-7}**	**−0.30**	**6.2×10^{-6}**	−0.040	0.12
wNA	**0.19**	**0.0060**	−0.050	0.43	0.010	0.83
cNA	−0.12	0.073	**−0.43**	**4.6×10^{-11}**	**−0.10**	**3.4×10^{-5}**
eNA	**−0.48**	**5.7×10^{-10}**	**−0.23**	**2.2×10^{-5}**	**−0.32**	**9.7×10^{-46}**
Europe	0.11	0.13	0.070	0.28	**−0.10**	3.3×10^{-5}
wAsia	0.10	0.16	0.12	0.075	−0.03	0.16
cAsia	**0.43**	3.2×10^{-11}	**−0.37**	**8.6×10^{-8}**	**0.080**	**0.0012**
eAsia	**0.14**	**0.033**	−0.030	0.64	**0.080**	**0.0011**

necessarily lead to a stronger midlatitude atmospheric response (Peings and Magnusdottir 2014).

The objective of this sensitivity study was to quantify the robustness of the atmospheric response to a systematically perturbed Arctic sea ice cover. We have shown using several different metrics that the remote atmospheric response can be nonrobust as a result of internal dynamics alone and leave diagnosis of mechanisms behind this nonrobustness for future studies. Here we can only speculate about possible reasons for the nonlinear behavior of the remote response. One conceivable explanation for the general decrease in extreme cold events in the −3 scenario with most severe sea ice loss is that the amplified warming in the Arctic leads to a larger warming of northerly winds compared with southerly winds, resulting in a reduced temperature variability in the mid- and high latitudes (Schneider et al. 2015; Screen 2014; Sun et al. 2015). We hypothesize that this direct thermal effect is especially important for the approximately linear decrease in the occurrence of extreme cold winter days in eastern North America with decreasing Arctic sea ice cover, largely because of the strong warming over the nearby Hudson Bay, consistent with the results of Screen et al. (2015a). In eastern Asia, the changes in frequency of extreme cold events were found to be more complex and related to a dynamical response that affects the general circulation of the atmosphere. The nonlinearity of the atmospheric circulation response, which bears some resemblance to the negative phase of the AO, could be due to a strong dependence of the response on the state of internal variability of the atmosphere. In other words, sea ice loss in the Arctic may be conducive to a more frequent negative AO-like circulation pattern in winter, but there could be other controlling factors involved, such as the background flow and the amplitude and phase of large-scale atmospheric waves. It is possible that 55 ensemble members (or equivalently 55 years of observations) for each Arctic sea ice state may represent an insufficient sample size to robustly distinguish this complex dynamical response from internal variability and that the apparent nonlinearity is caused by random sampling. Finally, we remark that two sea ice scenarios (−0.5 and especially −2) that displayed a relatively strong and statistically significant atmospheric response in the midlatitudes also exhibit a significant wintertime response in the stratosphere, with a deceleration and weakening of the stratospheric polar vortex, suggesting that upward-propagating planetary waves and their interference with climatological stationary waves could play a crucial role for the link between Arctic sea ice loss and changes in midlatitudes weather patterns, as has been proposed by some recent studies (Feldstein and Lee 2014; Kim et al. 2014; Peings and Magnusdottir 2014). More work is needed to understand these suggested pathways from the Arctic to the midlatitudes.

In conclusion, we have shown that Arctic sea ice loss can result in subsequent changes in midlatitude atmospheric circulations that resemble the negative phase of the AO and may increase the frequency of extreme cold winter events in eastern Asia, but these responses are not robust and are highly sensitive to the sea ice perturbations or atmospheric conditions. A small change in the sea ice perturbations or atmospheric conditions can lead to failure to capture these responses. Thus, this nonrobustness could explain some of the discrepancies between previous modeling studies. Our results suggest that the links between Arctic sea ice loss and changes in midlatitude weather patterns are not primarily through a direct response to the amplified warming in the Arctic and weakening of the meridional thickness gradient but involve more complex mechanisms that give rise to the strongly nonrobust behavior of the midlatitude atmospheric response.

Acknowledgments. We thank anonymous reviewers for constructive and helpful suggestions. We are also thankful to the Texas Advanced Computing Center (TACC) for providing us resources to perform the model simulations. The research is partially supported by the E. Willard and Ruby S. Miller Faculty Fellowship.

REFERENCES

Alexander, M. A., U. S. Bhatt, J. E. Walsh, M. S. Timlin, J. S. Miller, and J. D. Scott, 2004: The atmospheric response to realistic Arctic sea ice anomalies in an AGCM during winter. *J. Climate*, **17**, 890–905, doi:10.1175/1520-0442(2004)017<0890:TARTRA>2.0.CO;2.

Archer, C. L., and K. Caldeira, 2008: Historical trends in the jet streams. *Geophys. Res. Lett.*, **35**, L08803, doi:10.1029/2008GL033614.

Barnes, E. A., 2013: Revisiting the evidence linking Arctic amplification to extreme weather in midlatitudes. *Geophys. Res. Lett.*, **40**, 4734–4739, doi:10.1002/grl.50880.

——, and L. M. Polvani, 2015: CMIP5 projections of Arctic amplification, of the North American/North Atlantic circulation, and of their relationship. *J. Climate*, **28**, 5254–5271, doi:10.1175/JCLI-D-14-00589.1.

Berckmans, J., T. Woollings, M.-E. Demory, P.-L. Vidale, and M. Roberts, 2013: Atmospheric blocking in a high resolution climate model: Influences of mean state, orography and eddy forcing. *Atmos. Sci. Lett.*, **14**, 34–40, doi:10.1002/asl2.412.

Blackport, R., and P. J. Kushner, 2016: The transient and equilibrium climate response to rapid summertime sea ice loss in CCSM4. *J. Climate*, **29**, 401–417, doi:10.1175/JCLI-D-15-0284.1.

Cohen, J., and Coauthors, 2014: Recent Arctic amplification and extreme mid-latitude weather. *Nat. Geosci.*, **7**, 627–637, doi:10.1038/ngeo2234.

Comiso, J. C., C. L. Parkinson, R. Gersten, and L. Stock, 2008: Accelerated decline in the Arctic sea ice cover. *Geophys. Res. Lett.*, **35**, L01703, doi:10.1029/2007GL031972.

Deser, C., R. A. Tomas, M. Alexander, and D. Lawrence, 2010: The seasonal atmospheric response to projected Arctic sea ice loss in the late twenty-first century. *J. Climate*, **23**, 333–351, doi:10.1175/2009JCLI3053.1.

——, ——, and L. Sun, 2015: The role of ocean–atmosphere coupling in the zonal-mean atmospheric response to Arctic sea ice loss. *J. Climate*, **28**, 2168–2186, doi:10.1175/JCLI-D-14-00325.1.

Feldstein, S. B., and S. Lee, 2014: Intraseasonal and interdecadal jet shifts in the Northern Hemisphere: The role of warm pool tropical convection and sea ice. *J. Climate*, **27**, 6497–6518, doi:10.1175/JCLI-D-14-00057.1.

Francis, J. A., and S. J. Vavrus, 2012: Evidence linking Arctic amplification to extreme weather in mid-latitudes. *Geophys. Res. Lett.*, **39**, L06801, doi:10.1029/2012GL051000.

——, and ——, 2015: Evidence for a wavier jet stream in response to rapid Arctic warming. *Environ. Res. Lett.*, **10**, 014005, doi:10.1088/1748-9326/10/1/014005.

Franzke, C., and S. B. Feldstein, 2005: The continuum and dynamics of Northern Hemisphere teleconnection patterns. *J. Atmos. Sci.*, **62**, 3250–3267, doi:10.1175/JAS3536.1.

Gerber, F., J. Sedlek, and R. Knutti, 2014: Influence of the western North Atlantic and the Barents Sea on European winter climate. *Geophys. Res. Lett.*, **41**, 561–567, doi:10.1002/2013GL058778.

Gerdes, R., 2006: Atmospheric response to changes in Arctic sea ice thickness. *Geophys. Res. Lett.*, **33**, L18709, doi:10.1029/2006GL027146.

Honda, M., K. Yamazaki, H. Nakamura, and K. Takeuchi, 1999: Dynamic and thermodynamic characteristics of atmospheric response to anomalous sea-ice extent in the Sea of Okhotsk. *J. Climate*, **12**, 3347–3358, doi:10.1175/1520-0442(1999)012<3347:DATCOA>2.0.CO;2.

Hopsch, S., J. Cohen, and K. Dethloff, 2012: Analysis of a link between fall Arctic sea ice concentration and atmospheric patterns in the following winter. *Tellus*, **64A**, 18624, doi:10.3402/tellusa.v64i0.18624.

IPCC, 2013: *Climate Change 2013: The Physical Science Basis*. Cambridge University Press, 1535 pp., doi:10.1017/CBO9781107415324.

Jaiser, R., K. Dethloff, D. Handorf, A. Rinke, and J. Cohen, 2012: Impact of sea ice cover changes on the Northern Hemisphere atmospheric winter circulation. *Tellus*, **64A**, 11595, doi:10.3402/tellusa.v64i0.11595.

Johnson, N. C., S. B. Feldstein, and B. Tremblay, 2008: The continuum of Northern Hemisphere teleconnection patterns and a description of the NAO shift with the use of self-organizing maps. *J. Climate*, **21**, 6354–6371, doi:10.1175/2008JCLI2380.1.

Jung, T., and Coauthors, 2012: High-resolution global climate simulations with the ECMWF model in Project Athena: Experimental design, model climate, and seasonal forecast skill. *J. Climate*, **25**, 3155–3172, doi:10.1175/JCLI-D-11-00265.1.

Kim, B.-M., S.-W. Son, S.-K. Min, J.-H. Jeong, S.-J. Kim, X. Zhang, T. Shim, and J.-H. Yoon, 2014: Weakening of the stratospheric polar vortex by Arctic sea-ice loss. *Nat. Commun.*, **5**, 4646, doi:10.1038/ncomms5646.

Kinnard, C., C. M. Zdanowicz, D. A. Fisher, E. Isaksson, A. de Vernal, and L. G. Thompson, 2011: Reconstructed changes in Arctic sea ice over the past 1,450 years. *Nature*, **479**, 509–512, doi:10.1038/nature10581.

Kohonen, T., 1982: Self-organized formation of topologically correct feature maps. *Biol. Cybern.*, **43**, 59–69, doi:10.1007/BF00337288.

Li, C., B. Stevens, and J. Marotzke, 2015: Eurasian winter cooling in the warming hiatus of 1998–2012. *Geophys. Res. Lett.*, **42**, 8131–8139, doi:10.1002/2015GL065327.

Liu, J., J. A. Curry, H. Wang, M. Song, and R. M. Horton, 2012: Impact of declining Arctic sea ice on winter snowfall. *Proc. Natl. Acad. Sci. USA*, **109**, 4074–4079, doi:10.1073/pnas.1114910109.

Mori, M., M. Watanabe, H. Shiogama, J. Inoue, and M. Kimoto, 2014: Robust Arctic sea-ice influence on the frequent Eurasian cold winters in past decades. *Nat. Geosci.*, **7**, 869–873, doi:10.1038/ngeo2277.

Neale, R. B., and Coauthors, 2012: Description of the NCAR Community Atmosphere Model (CAM 5.0). NCAR Tech. Note NCAR/TN-486+STR, 289 pp. [Available online at http://www.cesm.ucar.edu/models/cesm1.0/cam/docs/description/cam5_desc.pdf.]

Oleson, K. W., and Coauthors, 2013: Technical description of version 4.5 of the Community Land Model (CLM). NCAR Tech. Note NCAR/TN-503+STR, 422 pp., doi:10.5065/D6RR1W7M.

Peings, Y., and G. Magnusdottir, 2014: Response of the wintertime Northern Hemisphere atmospheric circulation to current and projected Arctic sea ice decline: A numerical study with CAM5. *J. Climate*, **27**, 244–264, doi:10.1175/JCLI-D-13-00272.1.

Perlwitz, J., M. Hoerling, and R. Dole, 2015: Arctic tropospheric warming: Causes and linkages to lower latitudes. *J. Climate*, **28**, 2154–2167, doi:10.1175/JCLI-D-14-00095.1.

Petoukhov, V., and V. A. Semenov, 2010: A link between reduced Barents-Kara Sea ice and cold winter extremes over northern continents. *J. Geophys. Res.*, **115**, D21111, doi:10.1029/2009JD013568.

Polyak, L., and Coauthors, 2010: History of sea ice in the Arctic. *Quat. Sci. Rev.*, **29**, 1757–1778, doi:10.1016/j.quascirev.2010.02.010.

Porter, D. F., J. J. Cassano, and M. C. Serreze, 2012: Local and large-scale atmospheric responses to reduced Arctic sea ice and ocean warming in the WRF Model. *J. Geophys. Res.*, **117**, D11115, doi:10.1029/2011JD016969.

Rayner, N. A., 2003: Global analyses of sea surface temperature, sea ice, and night marine air temperature since the late nineteenth century. *J. Geophys. Res.*, **108**, 4407, doi:10.1029/2002JD002670.

Schneider, T., T. Bischoff, and H. Potka, 2015: Physics of changes in synoptic midlatitude temperature variability. *J. Climate*, **28**, 2312–2331, doi:10.1175/JCLI-D-14-00632.1.

Screen, J. A., 2014: Arctic amplification decreases temperature variance in northern mid- to high-latitudes. *Nat. Climate Change*, **4**, 577–582, doi:10.1038/nclimate2268.

——, and I. Simmonds, 2010: The central role of diminishing sea ice in recent Arctic temperature amplification. *Nature*, **464**, 1334–1337, doi:10.1038/nature09051.

——, and ——, 2013a: Caution needed when linking weather extremes to amplified planetary waves. *Proc. Natl. Acad. Sci. USA*, **110**, E2327–E2327, doi:10.1073/pnas.1304867110.

——, and ——, 2013b: Exploring links between Arctic amplification and mid-latitude weather. *Geophys. Res. Lett.*, **40**, 959–964, doi:10.1002/grl.50174.

——, and ——, 2014: Amplified mid-latitude planetary waves favour particular regional weather extremes. *Nat. Climate Change*, **4**, 704–709, doi:10.1038/nclimate2271.

——, ——, C. Deser, and R. Tomas, 2013: The atmospheric response to three decades of observed Arctic sea ice loss. *J. Climate*, **26**, 1230–1248, doi:10.1175/JCLI-D-12-00063.1.

——, C. Deser, I. Simmonds, and R. Tomas, 2014: Atmospheric impacts of Arctic sea-ice loss, 1979–2009: Separating forced change from atmospheric internal variability. *Climate Dyn.*, **43**, 333–344, doi:10.1007/s00382-013-1830-9.

——, ——, and L. Sun, 2015a: Reduced risk of North American cold extremes due to continued Arctic sea ice loss. *Bull. Amer. Meteor. Soc.*, **96**, 1489–1503, doi:10.1175/BAMS-D-14-00185.1.

——, ——, and ——, 2015b: Projected changes in regional climate extremes arising from Arctic sea ice loss. *Environ. Res. Lett.*, **10**, 084006, doi:10.1088/1748-9326/10/8/084006.

Semenov, V. A., and M. Latif, 2015: Nonlinear winter atmospheric circulation response to Arctic sea ice concentration anomalies for different periods during 1966–2012. *Environ. Res. Lett.*, **10**, 054020, doi:10.1088/1748-9326/10/5/054020.

Serreze, M. C., and J. A. Francis, 2006: The Arctic amplification debate. *Climatic Change*, **76**, 241–264, doi:10.1007/s10584-005-9017-y.

Simmonds, I., 2015: Comparing and contrasting the behaviour of Arctic and Antarctic sea ice over the 35 year period 1979–2013. *Ann. Glaciol.*, **56**, 18–28, doi:10.3189/2015AoG69A909.

——, and K. Keay, 2009: Extraordinary September Arctic sea ice reductions and their relationships with storm behavior over 1979–2008. *Geophys. Res. Lett.*, **36**, L19715, doi:10.1029/2009GL039810.

——, and P. D. Govekar, 2014: What are the physical links between Arctic sea ice loss and Eurasian winter climate? *Environ. Res. Lett.*, **9**, 101003, doi:10.1088/1748-9326/9/10/101003.

Sun, L., C. Deser, and R. A. Tomas, 2015: Mechanisms of stratospheric and tropospheric circulation response to projected Arctic sea ice loss. *J. Climate*, **28**, 7824–7845, doi:10.1175/JCLI-D-15-0169.1.

Tang, Q., X. Zhang, X. Yang, and J. A. Francis, 2013: Cold winter extremes in northern continents linked to Arctic sea ice loss. *Environ. Res. Lett.*, **8**, 014036, doi:10.1088/1748-9326/8/1/014036.

Taylor, K. E., D. Williamson, and F. Zwiers, 2000: The sea surface temperature and sea-ice concentration boundary conditions for AMIP II simulations. Program for Climate Model Diagnosis and Intercomparison Rep. 60, 28 pp.

Vihma, T., 2014: Effects of Arctic sea ice decline on weather and climate: A review. *Surv. Geophys.*, **35**, 1175–1214, doi:10.1007/s10712-014-9284-0.

Wallace, J. M., I. M. Held, D. W. J. Thompson, K. E. Trenberth, and J. E. Walsh, 2014: Global warming and winter weather. *Science*, **343**, 729–730, doi:10.1126/science.343.6172.729.

Walsh, J. E., 2014: Intensified warming of the Arctic: Causes and impacts on middle latitudes. *Global Planet. Change*, **117**, 52–63, doi:10.1016/j.gloplacha.2014.03.003.

Woollings, T., B. Harvey, and G. Masato, 2014: Arctic warming, atmospheric blocking and cold European winters in CMIP5 models. *Environ. Res. Lett.*, **9**, 014002, doi:10.1088/1748-9326/9/1/014002.

Yang, S., and J. H. Christensen, 2012: Arctic sea ice reduction and European cold winters in CMIP5 climate change experiments. *Geophys. Res. Lett.*, **39**, L20707, doi:10.1029/2012GL053338.